

H₂CO₃ Forms via HCO₃[−] in Water

András Stirling* and Imre Pápai

Chemical Research Center of the Hungarian Academy of Sciences, Budapest, Hungary

Received: October 18, 2010; Revised Manuscript Received: November 9, 2010

According to the generally accepted picture of CO₂ dissolution in water, the formation of H₂CO₃ proceeds in a single step that involves the attack of a water oxygen on the CO₂ carbon in concert with a proton transfer to a CO₂ oxygen. In the present work, a series of ab initio molecular dynamics simulations have been carried out along with the metadynamics technique which reveals a stepwise mechanism: the reaction of a water molecule with CO₂ yields HCO₃[−] as an intermediate and a hydronium ion, whereas the protonation of the CO₂ moiety occurs in a separate step representing a well-defined activation barrier toward the H₂CO₃ molecule. This alternative scenario was already taken into consideration decades ago, but subsequent experiments and calculations have given preference to the concerted mechanism. Employing extended periodic models of the CO₂–water system that mimic the bulk aqueous environment, the present simulations yield the complete free energy profile of the stepwise mechanism and provide a detailed microscopic mechanism of the elementary steps. HCO₃[−] formation is found to be the rate-determining step of the entire CO₂ hydration process.

I. Introduction

Gaseous carbon dioxide dissolves in water and a small fraction is converted into carbonic acid (H₂CO₃), which is in complex equilibrium with its dissociated forms (HCO₃[−] and CO₃^{2−}). This reversible hydration process is fundamental in various geochemical transformations,¹ and it plays a vital role in living organisms as well. The biologic CO₂ hydration is catalyzed by carbonic anhydrases, which enables efficient CO₂ transportation and pH regulation.^{2,3}

It has long been recognized that the nonenzymatic hydration of CO₂ can occur via two pathways.⁴ Under neutral or acidic conditions, the aqueous CO₂ is known to react directly with water to yield H₂CO₃, whereas at higher pH values (pH > 8), the reaction with OH[−] dominates and the prevailing products are HCO₃[−] and CO₃^{2−}. Given the importance of these reactions, they have been the subject of intensive kinetic^{5–16} and computational^{17–34} studies, but the detailed mechanistic interpretation of the role of water environment is not well-established.

For the water pathway, the kinetic data are usually analyzed in terms of Eigen's triangular scheme¹⁶ (see Figure 1), which assumes that the formation and decomposition of carbonic acid can occur either in a single step (eq 1 in Figure 1) or via the HCO₃[−] intermediate (eqs 2 and 3 in Figure 1).

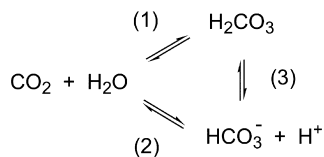


Figure 1. Eigen's triangular scheme.

Various experimental techniques have been employed to characterize the kinetics of the CO₂ reaction with water such as temperature variation,⁶ isotope exchange,^{5,9,12} pH change^{7,10,16} or stopped-flow studies.^{7,8,10,13,14} In a very recent study, a much

better temporal resolution has been achieved by following the H₂CO₃ formation by time-resolved femtosecond infrared spectroscopy.¹⁵ However, none of these studies could explicitly identify the exact sequence of the elementary steps leading to the formation of carbonic acid. The kinetics has been interpreted by tacitly assuming the concerted, one-step formation.

Theoretical studies aimed at providing further mechanistic details^{17–34} underline the catalytic role of water molecules and suggest that the formation of H₂CO₃ proceeds in a single step featuring the nucleophilic attack of H₂O on CO₂ coupled with an instantaneous proton relay via H-bonded water chain. The calculations have unequivocally demonstrated that as the number of H₂O molecules in the water chain is increasing, the activation barrier is decreasing.^{18,19,21,24,25,30,31,34} QCISD(T)/6-31G(d,)//MP2/6-31G(d,p) calculations in combinations with SCRF and PCM solvent models showed that four and three water molecules are necessary for CO₂ hydration in gas-phase and solution, respectively.¹⁹ CCSD(T)/aug-cc-pVDZ and CCSD(T)/aug-cc-pVTZ calculations have been used to calculate reaction rate using variational TST including quantum corrections and showed that the most favorable reaction route goes via a six-membered transition state.³⁰ Calculations at the MP4/6-311G(d,p)//MP2/6-31G(d,p) and QCISD(T)/6-31G(d,p)//MP2/6-31G(d,p) levels yielded an interesting conceptual insight into the mechanism: the most favorable proton-shuttle catalysis by a two-water proton chain and its hydration by a third water molecule coupled in a synergistic manner.³¹ CCSD(T)/CBS//MP2/aug-cc-pVTZ free energy calculations employing the PCM solvent model proposed that the most favorable route features a three-water chain. Additional water molecules can stabilize this transition structure by microsolvation.³⁴ Kumar et al. performed metadynamics calculations to simulate the finite temperature gas-phase decomposition of H₂CO₂ to CO₂ water.³³ In agreement with previous studies, they obtained a concerted reaction mechanism. Clearly, the problem of the above studies is that they employed computation models that are inherently biased for the proton-shuttle mechanism. In our present work, we carried out ab initio molecular dynamics simulations on extended

* To whom correspondence should be addressed. E-mail: stirling@chemres.hu.

models and our results indicate that the above generally accepted picture can be challenged.

II. Computational Methodology

The calculations have been performed within the Car–Parrinello molecular dynamics framework³⁵ as incorporated into the CPMD program package.³⁶ This approach enables us to capture the finite temperature effects of the system by sampling the classical atomic motions governed by forces obtained directly from quantum chemical calculations. The simulation model of the hydrated CO₂ consisted of 63 water molecules and a CO₂ molecule placed into a periodic box of $12.416 \times 12.416 \times 12.416 \text{ Å}^3$. Classical NPT simulations have been performed to obtain these cell parameters at ambient pressure ($\rho = 1.02 \text{ g/cm}^3$). The CO₂/H₂O ratio in this model corresponds to a 0.9 M concentration for all the calculated species (CO₂, HCO₃[−], and H₂CO₃). While for HCO₃[−] and H₂CO₃ this concentration is within the typical experimental range, for CO₂ this is somewhat higher, but we do not expect any change in its reactivity at this concentration. The initial configuration of atoms was obtained from further classical NVE simulation and subsequent equilibration for 2 ps with the quantum chemical setup. For the systems having HCO₃[−] and H₂CO₃ molecules, we started the simulations from the final configuration of the simulation yielding these species. In particular, the simulations of the reactions leading to either H₂CO₃ or CO₂ formation have been started from the final configuration of the simulation on the reaction $\text{CO}_2 + 2\text{H}_2\text{O}$, whereas the simulation on reaction $\text{H}_2\text{CO}_3 + \text{H}_2\text{O} \rightarrow \text{HCO}_3^- + \text{H}_3\text{O}^+$ has been started from the final configuration of the simulation on the H₂CO₃ formation. The limited size of the periodic box has important effects on the calculated energy values due to electrostatic and entropy-related reasons. These effects are estimated to amount to 1 kcal/mol, as described in the Supporting Information. We have employed the BLYP exchange-correlation functional³⁷ and ultrasoft pseudopotentials with a plane wave basis set expanded up to 27 Ry energy cutoff at the Γ point. The hydrogen atoms have been replaced by deuterium, which allowed 7 au time step for integrating the MD equations. In line with experiment, we do not expect variation in the reactivity due to deuteration.¹⁵ The fictitious electron mass was set to 700 au. The temperature of the simulations has been kept at 350 K employing the Nosé–Hoover thermostat, as previous studies indicated³⁸ that this temperature is needed to reproduce the 300 K behavior of water using the present simulation setup. Other simulation parameters have been tested as well; in particular, we have compared the BLYP and PBE³⁹ functionals and found that they yield very similar activation barriers for the reaction $\text{CO}_2 + 2\text{H}_2\text{O} \rightarrow \text{HCO}_3^- + \text{H}_3\text{O}^+$ (18.8 and 18.2 kcal/mol, respectively).

Reactive trajectories have been obtained by employing the metadynamics technique.^{40,41} This methodology has been proved to be very efficient in exploring reaction free energy surfaces (FES) in terms of general collective coordinates (CVs).⁴² The metadynamics has been extensively reviewed previously;⁴³ thus, we give only a brief summary of the method here. The spirit of the method is to introduce a history-dependent bias in the space of a few collective variables (CVs) $s_i(\mathbf{R})$ ($i \leq 3$ in this study). The CVs can be the functions of an arbitrary number of atomic coordinates (\mathbf{R}), and the reaction free energy is sampled in the space spanned by these CVs. We have selected coordination numbers (CNs) and distances as CVs. In particular, we chose the CVs of the actual simulations from the following set: CV₁, the number of water oxygen atoms bonded to the carbon atom; CV₂, number of hydrogen atoms bonded to the carbonate oxygen

atoms; CV₃, the distance of the hydronium ion from the oxygen atoms bonded to the carbon atom; and CV₄, the number of the H-bonds formed by a hydronium ion if present. The selected CVs account for the underlying chemical changes, namely, the C–O bond formation (CV₁), the proton exchange with water (CV₂), the migration of the hydronium ion (CV₃), and its solvation structure (CV₄). The last three CVs have already been successfully applied in describing the dissociation of acetic acid.⁴⁵

In this study, the simulations have been carried out until the first barrier crossing. The corresponding back reactions were simulated separately. This strategy allowed us to define more appropriate CV sets for each simulation and required shorter simulation times. Note that metadynamics with several recrossings yields more accurate free energy surfaces but requires much longer CPU time; hence, quantum chemical metadynamics simulations are often conducted following this strategy (e.g., refs 45–49). The error of such single metadynamics profiles has been estimated to be 1.5 kcal/mol following refs 41, 43, and 44. The metadynamics runs reconstructed the FES of the initial minima (reactant regions) up to the barrier when the system starts to explore the product region of the simulated reaction path, and the product regions were scanned only partially by the metadynamics bias potential. We note that in the present context *reactant* and *product* regions refer to the initial and final states of a single reaction path and not to the left and right sides of an equilibrium. For each equilibrium, we have therefore performed separate simulations for the forward and the backward routes and obtained two FES featuring the calculated free energy well of the initial state of each process. The relative stability of reactants and products has been estimated from the calculated activation barriers. Further details of the metadynamics, the analytic form of the CVs, description of our metadynamics protocol, the parameters used in the simulations, the error sources, their estimated size and all the calculated FES can be found in the Supporting Information.

III. Results

As a first step in exploring the reaction mechanism of CO₂ hydration, the attack of a water molecule on CO₂ has been investigated. The set of CVs employed here (CV₁, CV₂) guided both the approach of H₂O to CO₂ and the protonation of the oxygens of CO₂. The simulations revealed that the C–O bond formation is coupled with a proton transfer from the attacking H₂O to nearby waters, generating HCO₃[−] and H₃O⁺. Along this pathway, a water molecule coordinates to the carbon of the CO₂ molecule, and after overcoming the barrier of the C–O bond formation (around 6 ps), the attacking H₂O releases spontaneously a proton to the solvent, yielding HCO₃[−]. The hydronium ion formed in this way is transferred rapidly to nearby water molecules via structural diffusion but remains within a short distance from the HCO₃[−] in terms of hydrogen-bond wires during the next picoseconds.⁵⁰ The most remarkable feature of the HCO₃[−] formation is this strictly asynchronous proton detachment occurring spontaneously after the reaction went through the barrier. The simulations also show that hydrogen-bond wires of various lengths can form between the attacking water molecules and the oxygen moiety, but a complete proton transfer along these wires does not take place during the simulation. In Figure 2, we show the temporal formations of H-bonded water chains of three different lengths along with the evolution of the CVs.⁵¹ We can see that their formation has no correlation with the variation of CV₁, while their presence and large CV₂ values appear simultaneously.⁵³ Figure 2 also shows that such

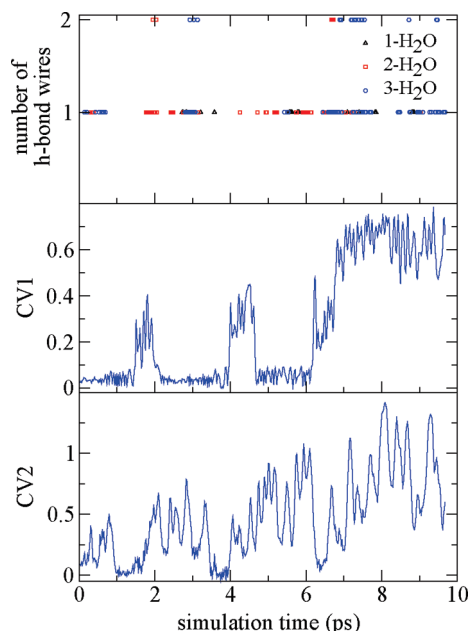


Figure 2. Temporal formation of H-bond wire between the attacking water molecule (defined as the closest to the CO₂ carbon) and the oxygen atoms of CO₂. The triangles, squares, and circles label the lengths of the connecting H-bonded water chains. The graph also shows the evolution of CV₁ and CV₂. We note that H-bond wires longer than three can also be observed in increasing frequencies.

TABLE 1: Calculated and Experimental Activation Free Energies^a (kcal/mol)

reaction step	$F_{\text{act}}^{\text{theor}}$	$F_{\text{act}}^{\text{exp}}$
$\text{CO}_2 + 2\text{H}_2\text{O} \rightarrow \text{HCO}_3^- + \text{H}_3\text{O}^+$	18.8	21.8 ^{b,c}
$\text{HCO}_3^- + \text{H}_3\text{O}^+ \rightarrow \text{CO}_2 + 2\text{H}_2\text{O}$	10.4	10.6 ^b
$\text{HCO}_3^- + \text{H}_3\text{O}^+ \rightarrow \text{H}_2\text{CO}_3 + \text{H}_2\text{O}$	4.4	
$\text{H}_2\text{CO}_3 + \text{H}_2\text{O} \rightarrow \text{HCO}_3^- + \text{H}_3\text{O}^+$	9.5	

^a Helmholtz and Gibbs free energies, respectively. See also the Supporting Information. ^b Reference 14. ^c The experiment assumed direct H₂CO₃ formation from CO₂. On the basis of our calculated free energy profile, the HCO₃[−] formation is the rate-limiting step; therefore, we associate the experimental value to this step.

water wires can occur at any stage of the reaction, in particular at the TS. From gas-phase calculations it is already known that H-bond chains at the TS drive the reaction toward the concerted

H₂CO₃ formation.^{18,19,21,24,25,30,31,34} It follows, therefore, that the presence of the solvent has an important effect on the mechanism and opens up a stepwise channel.

The calculated activation free energy of this step is 18.8 kcal/mol. This is in reasonable agreement with the experimental 21.8 kcal/mol value (Table 1) if we take into consideration the error of the simulations and the limitations of the quantum chemistry setup. It thus appears that the reaction of CO₂ with water begins with bicarbonate formation. These observations also indicate that the $\text{CO}_2 + 2\text{H}_2\text{O} \rightarrow \text{HCO}_3^- + \text{H}_3\text{O}^+$ step can be in fact followed via a single CV. Additional 1D metadynamics runs employing only CV₁ yielded exactly the same path for this step. Deprotonation takes place spontaneously after barrier crossing. It is important to note that H-bond wires between the attacking water molecule and the oxygens of CO₂ could also be observed during the 1D metadynamics simulations (see the Supporting Information for details).

In Figure 3, three atomic configurations along the 1D metadynamics trajectory are depicted, which illustrate the mechanism of HCO₃[−] formation. The most important structural change in CO₂ activation is the bending of the molecule. The C–O dative bond formation corresponds to an electron transfer from the H₂O molecule to the CO₂ triggering this bending.⁵⁴ Figure 4 shows that the variation of CV₁ and the bending of the CO₂ molecule correlate well. Indeed, as the coordination of the H₂O becomes stronger, the bending is more pronounced. The electron transfer and the bending drastically change the total dipole moment of the CO₂ molecule.⁵⁵ The C–O bond formation takes place when the CO₂ is significantly bent (ca. 150°) and features a large dipole moment (fluctuating around 4–5 D; see Figure 4). The hydrate shell of the CO₂ molecule should adapt to this significant change in the charge distribution. The free energy barrier, therefore, involves the work to bend the CO₂ molecule against the electric field of the solvent cage and to form the C–O bond by electron donation from the attacking H₂O molecule.

After leaving the free energy barrier, the zwitterionic H₂O⁺CO₂[−] species transfers spontaneously a proton to a nearby water molecule (Figure 3C). The driving force of this process is the increased acidity of the coordinating water ligand due to its electron transfer to CO₂. The hydrogen bonds of the coordinating H₂O shorten as the reaction proceeds, indicating that the polarized solvent cage and the enhanced hydrogen bondings mediate the spontaneous proton dissociation. In Figure 5, we display the temporal variation of the OH bond lengths in the attacking H₂O molecule and the distances between the O

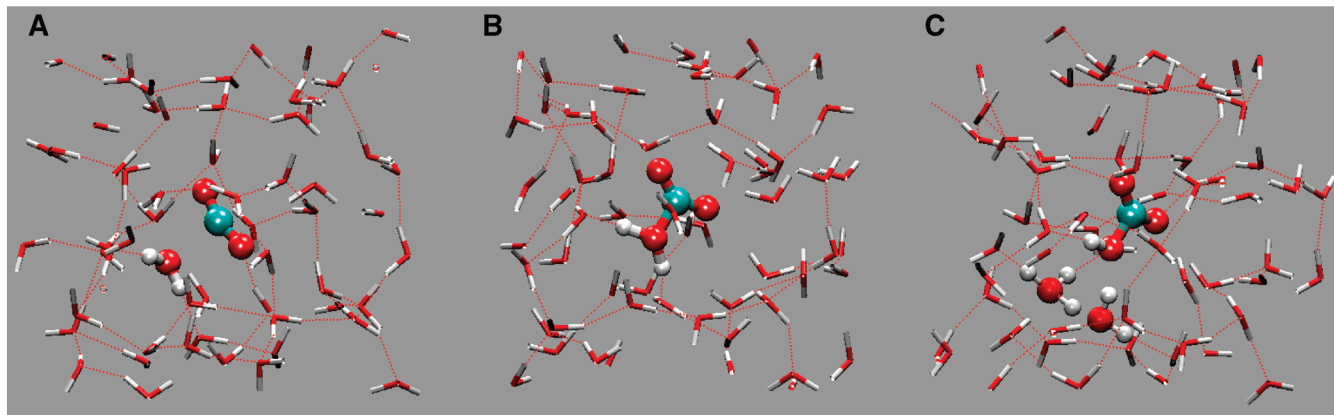


Figure 3. Snapshots of HCO₃[−] formation along the metadynamics trajectory: (A) the approach of H₂O to CO₂, (B) typical TS configuration, and (C) proton migration to solvent. Reacting atoms are shown in ball-and-stick representation, and the other solvent molecules are represented with simple tubes. Fragments occur due to periodic boundary conditions. Note that fragment H atoms are not shown.

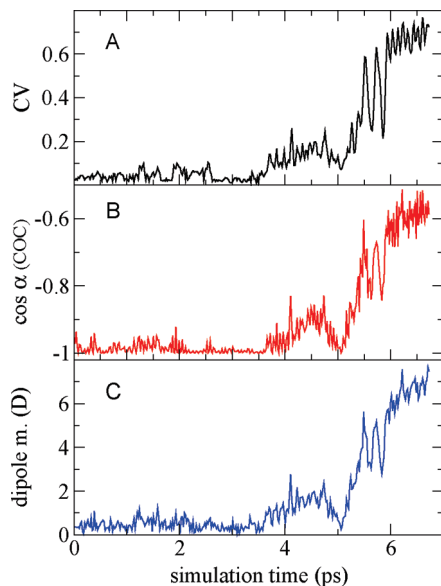


Figure 4. Time evolution of the reaction coordinate (A), the bond angle (B), and the dipole moment (C) of CO₂ upon the formation of HCO₃[−].

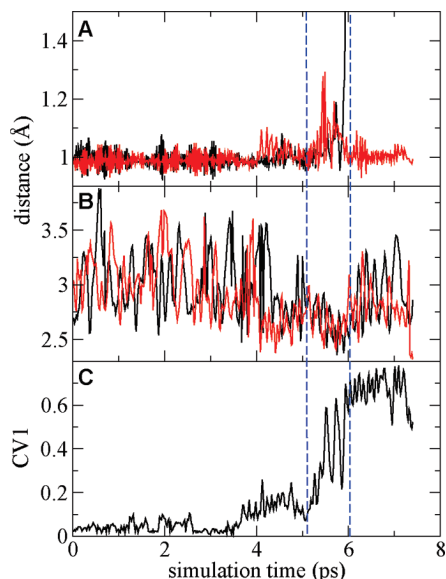


Figure 5. (A) Evolution of the two O–H bond lengths in the attacking water molecule. Note that one of the H atoms dissociates (black curve) and leaves the water ligand. The other H atom remains bonded to the bicarbonate ion (red curve). (B) Evolution of the O–O distances between the attacking water and its two H-bond acceptor neighbors (black and red curves). (C) Evolution of the reaction coordinate. Blue dashed lines indicate the TS region.

atom of this H₂O and its two H-bond acceptor water neighbors, along with the evolution of the reaction coordinate in the 1D metadynamics simulation. The graphs clearly show that as the reaction course reaches the TS region, the OH bonds elongate (Figure 5A) and the H-bonds become stronger (Figure 5B).

This barrierless charge separation leads the system into a free energy minimum. Hence, the hydronium and HCO₃[−] ions cannot recombine, neither can H₂CO₃ form promptly. The OH group in HCO₃[−] is a much weaker base than H₂O, while the protonation of the CO₂ moiety requires proton diffusion via a proton wire, which necessitates proper solvent fluctuations and activation energy.⁵⁶ This is in perfect agreement with recent experimental findings.⁵⁷ Infrared measurements of hydrated HCO₃[−] anion with up to 10 water molecules showed that

hydrogen bonding with the hydroxyl group is particularly disfavored, whereas the negatively charged CO₂ moiety of HCO₃[−] ion has a very strong preference for hydrogen bondings.

In accordance with the mechanism discussed above, in the reverse process (dehydration of HCO₃[−]), both the proton uptake and the C–O bond breaking contribute to the activation energy. Indeed, the metadynamics simulations carried out with the CV₁, CV₂, CV₃ set⁵⁸ showed the following sequence: first the hydronium ion transferred a proton to the hydroxyl group of the bicarbonate ion, forming a coordinated water (around 24 ps), which then dissociated from the CO₂ part of the molecule (around 26 ps). The predicted pathway has a 10.6 kcal/mol activation barrier, which is in excellent agreement with the experimental value (10.5 kcal/mol) derived from equilibrium and kinetic measurements.⁵⁹ The reaction free energy obtained from the activation energies is in fair agreement with experiment (8.4 vs 11.2 kcal/mol).

The recombination of HCO₃[−] and H₃O⁺ ions can also lead to H₂CO₃ via a proton transfer mechanism. Unbiased simulations showed that even in this relatively small unit cell, the lifetime of the H₃O⁺–HCO₃[−] ion pair without recombination can be on the order of a few picoseconds. Note, however, that the barrier of a single proton transfer is on the order of $k_B T$ (e.g., refs 56, 60), implying that configurational entropy plays an important role in stabilizing the dissociated state. Proton transfer can be actually observed during normal Car–Parrinello simulations as well. However, formation of H₂CO₃ requires the presence of a suitable proton wire along which the proton can be transferred to either oxygen atom of the CO₂ moiety of the bicarbonate ion. The simulations using the CV₂, CV₃, CV₄ set showed a large hydronium mobility⁶⁰ preceding the proton attachment to the bicarbonate ion. We found that the maximum size of the shortest H-bond path between the hydronium ion and the bicarbonate oxygen atoms is three water molecules in the dissociated state. The calculated activation free energy is 4.4 kcal/mol for the H₂CO₃ formation. The reverse process, i.e. the dissociation of H₂CO₃ (CV₂, CV₃, CV₄), features a higher energy barrier (9.5 kcal/mol). Inspection of the metadynamics trajectory shows that the proton transfer takes place around 4.9 ps following the mechanism already observed for the dissociation of acetic acid.⁴⁵ First, temporal contact ion pair formations could be seen at 2 and 3.7 ps between one of the protons of H₂CO₃ and a nearby water molecule which was H-bonded at the reactant state. The contact ion pairs rearrange to the normal neutral state within 0.4 ps by transferring back the proton to the HCO₃[−]. At the TS, the reaction goes through the contact ion pair state and the hydronium rapidly separates from the bicarbonate ion. Both the contact ion pair formation and the dissociation are triggered by a change in the H-bond structure of the proton-accepting water molecule: due to solvent fluctuations, this water molecule loses one of the H-bonds of its first solvation shell and can thus host the dissociating proton and become a hydronium ion.

The predicted free energy of the first dissociation step of H₂CO₃ is thus 5.1 kcal/mol, which corresponds to a pK_a of 3.7, in agreement with experiment.¹⁴ From the entire set of computed activation energies, we can also estimate the free energy of the H₂CO₃ formation from CO₂ and water. The calculated 3.3 kcal/mol value is satisfactorily close to the experimental 6.2 kcal/mol value.¹⁴

Our results presented above clearly suggest that a stepwise mechanism is operative in the CO₂ hydration process. The calculated free energy profile for the entire reaction is displayed in Figure 6. The first step of the hydration corresponds to the

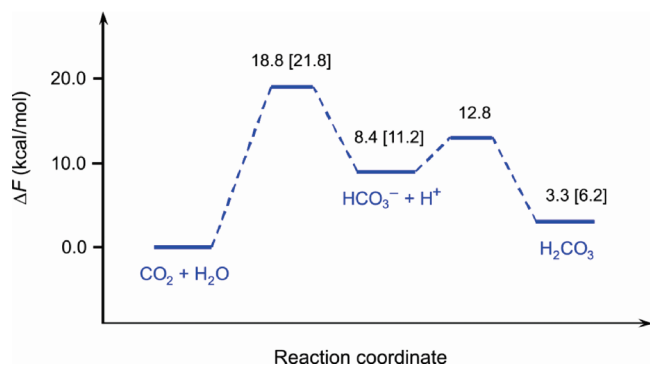


Figure 6. Calculated free energy profile of the formation of H_2CO_3 from CO_2 . Experimental data¹⁴ are given in brackets.

addition of H_2O to CO_2 , yielding HCO_3^- and a hydronium ion, and the formation of H_2CO_3 takes place in a subsequent step. The HCO_3^- formation has been found to be the rate-determining step. The typical textbook picture of the H_2CO_3 formation in a single concerted step⁶¹ could not be observed, although H-bonded water wire formation occurs at the TS, but without the necessary proton relay along it.

IV. Conclusions

Metadynamics simulations employing quantum chemical forces have been employed to obtain mechanistic insights into the CO_2 hydration process. From our calculations, a stepwise mechanism emerged, where the HCO_3^- formation precedes the formation of H_2CO_3 . The present findings have important implications. For instance, our results may provide new information for the interpretation of kinetic measurements that assumed the one-step formation of H_2CO_3 and the rate laws associated with the decomposition of H_2CO_3 . In particular, we underline the fact that neither the formation nor the decomposition of H_2CO_3 is an elementary step; hence, further experimental analysis of the kinetic data might be useful in this respect. Second, the kinetic stability of H_2CO_3 demonstrated experimentally in various ways^{15,17,18,30} can be readily explained by the consecutive steps forming the overall decomposition process. The present mechanism also supports the recent observation that the main cause of H_2CO_3 instability is acid dissociation.¹⁵ Finally, we also point out that in the light of the present findings, the uncatalyzed CO_2 hydration and enzyme-catalyzed CO_2 capture in living organisms follow the same pathway. Carbonic anhydrase enzymes have thus evolved to accelerate the bicarbonate formation, instead of inventing a new CO_2 hydration route to sidestep the direct H_2CO_3 formation assumed for the uncatalyzed CO_2 hydration.

Acknowledgment. We thank G. Schubert and I. Bakó for useful interactions. We thank Dr. Jung Mee Park for providing us with the implementation of CV₃ and CV₄. This work has been supported by OTKA Grants K-60549, K-81927, and K-68360. A large part of the calculations have been performed on the resources of NIIF. We thank Péter Stefán at NIIF for technical assistances. The anonymous referees are acknowledged for their constructive criticisms and insightful comments.

Supporting Information Available: Detailed description of the metadynamics technique, the definition of the CVs, the metadynamics parameters, the metadynamics protocol employed in the study, the error estimation procedure, the additional error sources, the H-bond wire evolution for the 1D simulation of reaction $\text{CO}_2 + 2\text{H}_2\text{O} \rightarrow \text{HCO}_3^- + \text{H}_3\text{O}^+$, and the calculated

free energy surfaces. This information is available free of charge via the Internet at <http://pubs.acs.org>.

References and Notes

- (1) (a) Lackner, K. L. *Annu. Rev. Energy Environ.* **2002**, 27, 193–232. (b) Hoegh-Guldberg, O.; Mumby, P. J.; Hooten, A. J.; Steneck, R. S.; Greenfield, P.; Gomez, E.; Harvell, C. D.; Sale, P. F.; Edwards, A. J.; Caldeira, K.; Knowlton, N.; Eakin, C. M.; Iglesias-Prieto, R.; Muthiga, N.; Bradbury, R. H.; Dubi, A.; Hatzioiols, M. E. *Science* **2007**, 318, 1737–1742.
- (2) (a) Lindsog, S. *Pharmacol. Ther.* **1997**, 74, 1–20. (b) Christianson, D. W.; Fierke, C. A. *Acc. Chem. Res.* **1996**, 29, 331–339. (c) Silverman, D. N.; McKenna, R. *Acc. Chem. Res.* **2007**, 40, 669–675.
- (3) Badger, M. R.; Price, G. D. *Annu. Rev. Plant. Physiol. Plant Mol. Biol.* **1994**, 45, 369–392.
- (4) Kern, D. M. *J. Chem. Educ.* **1960**, 37, 14–23.
- (5) Mills, G. A.; Urey, H. C. *J. Am. Chem. Soc.* **1940**, 62, 1019–1026.
- (6) Roughton, F. J. W. *J. Am. Chem. Soc.* **1941**, 63, 2930–2934.
- (7) Ho, C.; Sturtevant, J. M. *J. Biol. Chem.* **1963**, 238, 3499–3501.
- (8) Gibbons, B. H.; Edsall, J. T. *J. Biol. Chem.* **1963**, 238, 3502–3507.
- (9) Welch, M. J.; Lifton, J. F.; Seck, J. A. *J. Phys. Chem.* **1969**, 73, 3351–3356.
- (10) Pocker, Y.; Bjorquist, D. W. *J. Am. Chem. Soc.* **1977**, 99, 6537–6543.
- (11) Johnson, K. S. *Limnol. Oceanogr.* **1982**, 27, 849–855.
- (12) (a) Marlier, J. F.; O’Leary, M. H. *J. Am. Chem. Soc.* **1984**, 106, 5054–5057. (b) Paneth, P.; O’Leary, M. H. *J. Am. Chem. Soc.* **1985**, 107, 7381–7384.
- (13) Soli, A. L.; Byrne, R. H. *Mar. Chem.* **2002**, 78, 65–73.
- (14) Wang, X.; Conway, W.; Burns, R.; McCann, N.; Maeder, M. J. *Phys. Chem. A* **2010**, 114, 1734–1740.
- (15) Adamczyk, K.; Prémont-Schwarz, M.; Pines, D.; Pines, E.; Nibbering, E. T. J. *Science* **2009**, 326, 1690–1694.
- (16) Eigen, M.; Kustin, K.; Maass, G. *Z. Phys. Chem.* **1961**, 30, 130.
- (17) Hage, W.; Liedl, K. R.; Hallbrucker, A.; Mayer, E. *Science* **1998**, 279, 1332–1335.
- (18) Loerting, T.; Tautermann, C.; Koemer, R. T.; Kohl, I.; Hallbrucker, A.; Mayer, E.; Liedl, K. R. *Angew. Chem., Int. Ed.* **2000**, 39, 891–894.
- (19) Nguyen, M. T.; Raspoet, G.; Vanquickenborne, L.; Van Duijn, P. T. *J. Phys. Chem. A* **1997**, 101, 7379–7388.
- (20) Jönsson, B.; Karlström, G.; Wennerström, H.; Forsén, S.; Roos, B.; Almlöf, J. *J. Am. Chem. Soc.* **1977**, 99, 4628–4632.
- (21) Nguyen, M. T.; Ha, T.-K. *J. Am. Chem. Soc.* **1984**, 106, 599–602.
- (22) Buckingham, A. D.; Handy, N. C.; Rice, J. E.; Somasundram, K.; Dijkgraaf, C. *J. Comput. Chem.* **1986**, 7, 283–293.
- (23) Liang, J.-Y.; Lipscomb, W. L. *J. Am. Chem. Soc.* **1986**, 108, 5051–5058.
- (24) Nguyen, M. T.; Hegarty, A. F.; Ha, T.-K. *J. Mol. Struct. (THEOCHEM)* **1987**, 150, 319–325.
- (25) Merz, K. M., Jr. *J. Am. Chem. Soc.* **1990**, 112, 7973–7980.
- (26) Tachibana, A.; Fueno, H.; Tanaka, E.; Murashima, M.; Koizumi, M.; Yamabe, T. *Int. J. Quantum Chem.* **1991**, 39, 561–583.
- (27) Peng, Z.; Merz, K. M., Jr. *J. Am. Chem. Soc.* **1993**, 115, 9640–9647.
- (28) Wight, C. A.; Bolyrev, A. I. *J. Phys. Chem.* **1995**, 99, 12125–12130.
- (29) Liedl, K. R.; Sekušak, S.; Mayer, E. *J. Am. Chem. Soc.* **1997**, 119, 3782–3784.
- (30) Tautermann, C.; Voegelé, A. F.; Loerting, T.; Kohl, I.; Hallbrucker, A.; Mayer, E.; Liedl, K. R. *Chem.—Eur. J.* **2002**, 8, 66–73.
- (31) Lewis, M.; Glaser, R. *J. Phys. Chem. A* **2003**, 107, 6814–6818.
- (32) Jena, N. R.; Mishra, P. C. *Theor. Chem. Acc.* **2005**, 114, 189–199.
- (33) Kumar, P. P.; Kalinichev, A. G.; Kirkpatrick, R. J. *J. Chem. Phys.* **2007**, 126, 204315.
- (34) Nguyen, M. T.; Matus, M. H.; Jackson, V. E.; Ngan, V. T.; Rustad, J. R.; Dixon, D. A. *J. Phys. Chem. A* **2008**, 112, 10386–10398.
- (35) Car, R.; Parrinello, M. *Phys. Rev. Lett.* **1985**, 55, 2471–2474.
- (36) CPMD v3.11. Copyright IBM Corp 1990–2007, Copyright MPI für Festkörperforschung Stuttgart, 1997–2001.
- (37) (a) Becke, A. D. *Phys. Rev. A* **1988**, 38, 3098–3100. (b) Lee, C.; Yang, W.; Parr, R. G. *Phys. Rev. B* **1988**, 37, 785–789.
- (38) (a) Schwegler, E.; Grossman, J. C.; Gygi, F.; Galli, G. *J. Chem. Phys.* **2004**, 121, 5400–5409. (b) Fernández-Serra, M. V.; Artacho, E. *J. Chem. Phys.* **2004**, 121, 11136–11144.
- (39) Perdew, J. P.; Burke, K.; Ernzerhof, M. *Phys. Rev. Lett.* **1996**, 77, 3865–3868. Perdew, J. P.; Burke, K.; Ernzerhof, M. *Phys. Rev. Lett.* **1997**, 78, 1396.
- (40) (a) Laio, A.; Parrinello, M. *Proc. Natl. Acad. Sci. U.S.A.* **2002**, 99, 12562–12566. (b) Iannuzzi, M.; Laio, A.; Parrinello, M. *Phys. Rev. Lett.* **2003**, 90, 238302.
- (41) Laio, A.; Rodriguez-Fora, A.; Gervasio, F. L.; Ceccarelli, M.; Parrinello, M. *J. Phys. Chem. B* **2005**, 109, 6714–6721.

- (42) For selected examples, see: (a) Ensing, B.; Laio, A.; Gervasio, F. L.; Parrinello, M.; Klein, M. *J. Am. Chem. Soc.* **2004**, *126*, 9492–9493. (b) Stirling, A.; Iannuzzi, M.; Laio, A.; Parrinello, M. *ChemPhysChem* **2004**, *5*, 1558–1568. (c) Boero, M.; Ikeshoji, T.; Liew, C. C.; Terakura, K.; Parrinello, M. *J. Am. Chem. Soc.* **2004**, *126*, 6280–6286. (d) Ensing, B.; Klein, M. *Proc. Natl. Acad. Sci. U.S.A.* **2005**, *102*, 6755–6759. (e) Stirling, A.; Iannuzzi, M.; Parrinello, M.; Molnar, F.; Bernhart, V.; Luinstra, G. *Organometallics* **2005**, *24*, 2533–2537. (f) Nair, N. N.; Schreiner, E.; Marx, D. *J. Am. Chem. Soc.* **2006**, *128*, 13815–13826. (g) Blumberger, J.; Ensing, B.; Klein, M. *Angew. Chem., Int. Ed.* **2006**, *45*, 2893–2897. (h) Gervasio, F. L.; Boero, M.; Parrinello, M. *Angew. Chem., Int. Ed.* **2006**, *45*, 5606–5609. (i) Stanton, C. L.; Kuo, I-F. W.; Mundy, C. J.; Laino, T.; Houk, K. N. *J. Phys. Chem. B* **2007**, *111*, 12573.
- (43) (a) Laio, A.; Parrinello, M. *Lect. Not. Phys.* **2006**, *707*, 315–347. (44) (b) Laio, A.; Gervasio, F. L. *Rep. Prog. Phys.* **2008**, *71*, 126601. Bussi, G.; Laio, A.; Parrinello, M. *Phys. Rev. Lett.* **2006**, *96*, 090601.
- (45) Park, J. M.; Laio, A.; Iannuzzi, M.; Parrinello, M. *J. Am. Chem. Soc.* **2006**, *128*, 11318–11319.
- (46) Gunaydin, H.; Houk, K. N. *J. Am. Chem. Soc.* **2008**, *130*, 15232–15233.
- (47) Rodríguez-Fortea, A.; Vila-Nadal, L.; Poblet, J. M. *Inorg. Chem.* **2008**, *47*, 7745–7750.
- (48) Alfonso-Prieto, M.; Biarnés, X.; Vidossich, P.; Rovira, C. *J. Am. Chem. Soc.* **2009**, *131*, 11751–11761.
- (49) Comas-Vives, A.; Stirling, A.; Ujaque, G.; Lledos, A. *Chem.—Eur. J.* **2010**, *16*, 8738–8747.
- (50) After having crossed the barrier, the simulation have been conducted only for a few picoseconds.
- (51) For defining the proton wire, we used structural criteria as described in ref 52. For the presence of a H-bond between two water molecules, we calculated the h_{ij} function as a product of two terms:

$$h_{ij} = \frac{1 - \left(\frac{r_{ij} - C}{r_O}\right)^{10}}{1 - \left(\frac{r_{ij} - C}{r_O}\right)^{20}} \sum_k \frac{1 - \left(\frac{r_{ik} + r_{jk} - r_{ij}}{r_H}\right)^8}{1 - \left(\frac{r_{ik} + r_{jk} - r_{ij}}{r_H}\right)^{12}}$$

where $C = 2.7$ Å, $r_O = 0.5$ Å, and $r_H = 0.6$ Å. The first term is nonvanishing if the distance between the O_i and O_j atoms of the two water molecules is smaller than 3.5 Å and takes the maximal value of 1 when it is around 2.7 Å. The second term is 1 if O_iH_k + O_jH_k–O_iO_j is 0 and gradually vanishes as this sum exceeds 0.6. To locate the presence of a H-bond wire between the attacking water molecule and the oxygens of CO₂, we calculate the products $h_{ij}h_{ij}h_{jc}$, $h_{ij}h_{ij}h_{jk}h_{kc}$, and $h_{ij}h_{ij}h_{jk}h_{kl}h_{lc}$, where i is the index of the water closest to the carbon atom, i, j, k , and l run over the water oxygens (but $j \neq i$, $k \neq i, j$, and $l \neq i, j, k$), and, finally, c runs over the indices of the CO₂ oxygens. We accept the proton wire if the products are larger than 0.8. In this way, we can locate the presence of H-bond wire of length two, three, and four in terms of H-bond.

(52) Donadio, D.; Raiteri, P.; Parrinello, M. *J. Phys. Chem B* **2005**, *109*, 5421–5424.

(53) Note, however, that CV₂ can have a large value without a H-bond chain, as follows from its definition.

(54) Leitner, W. *Coord. Chem. Rev.* **1996**, *153*, 257–284.

(55) The dipole moment of a molecule in solution can be estimated from the Wannier centers and the atomic positions: Silvestrelli, P. L.; Bernasconi, M.; Parrinello, M. *Chem. Phys. Lett.* **1997**, *277*, 478–482.

(56) Geissler, P. L.; Dellago, C.; Chandler, D.; Hutter, J.; Parrinello, M. *Science* **2001**, *291*, 2121–2124.

(57) Garand, E.; Wende, T.; Goebbort, D. J.; Bergmann, R.; Meijer, G.; Neumark, D. M.; Asmis, K. R. *J. Am. Chem. Soc.* **2010**, *132*, 849–856.

(58) The role of CV₂ is only to prevent the H₂CO₃ formation by restraining the actual CNs at low values. See the Supporting Information for details.

(59) The 10.5 kcal/mol value has been derived using the experimental K_1 (eq 1, Figure 1) and K_{a2} (eq 2, Figure 1) equilibrium constants and the activation free energy value measured for k_1 at 25.0 °C in ref 14.

(60) Marx, D. *ChemPhysChem* **2006**, *7*, 1848–1870.

(61) Greenwood, N. N.; Earnshaw, A. *Chemistry of the Elements*; Butterworth/Heinemann: Oxford, 1997.

JP1099909